DINAME 2017 - Proceedings of the XVII International Symposium on Dynamic Problems of Mechanics
A. T. Fleury, D. A. Rade, P. R. G. Kurka (Editors), ABCM, São Sebastião, SP, Brazil, March 5-10, 2017

CHAOS CONTROL OF AN SMA-PENDULUM SYSTEM

Dimitri D. A. Costa[1], Marcelo A. Savi[1]

[1] Center for Nonlinear Mechanics, COPPE - Department of Mechanical Engineering
Universidade Federal do Rio de Janeiro
21.941.972 – Rio de Janeiro – RJ, Brazil, P.O. Box 68.503
dimitri.d.costa@gmail.com, savi@mecanica.ufrj.br

Abstract: Chaos control is usually employed to get advantage of the chaotic behavior stabilizing unstable periodic orbits embedded on the attractor. This paper deals with the chaos control applied to an SMA-Pendulum system. The system is composed by a pendulum excited by a string-spring-motor where the spring is built with shape memory alloys. The inclusion of smart material elements confers temperature dependent behavior that can be exploited for control purposes. Time delayed feedback control is employed as a controller using Floquet theory to estimate controller parameters. Temperature is employed as a control parameter considering asymmetric heat-cooling speeds. Numerical simulations show that the controller is able to perform chaos control.

Keywords: Nonlinear Dynamics, Chaos Control, Shape Memory Alloys.

INTRODUCTION

Pendulum systems are extensively studied on applied nonlinear dynamics and engineering, serving as models for a variety of systems like ankles (Suzuki *et al.*, 2012), electrical motors (Chen *et al.*, 2014), cranes (Ju *et al.*, 2006), and torsional dampers (Monroe and Shaw, 2013). De Paula *et al.* (2006) discussed some aspects of pendulum dynamics, presenting an experimental-numerical investigation of a typical mechanical apparatus. Results show several complex responses that include bifurcations, chaos and transient chaos. Nonlinear control of these systems are reported in several works, and it should be highlighted the use of either neural networks or chaos control approaches (Bessa *et al.*, 2009; de Paula and Savi, 2009; Pan *et al*., 2013).

The first continuous chaos control protocol was proposed by Pyragas (1992) and latter extended by Socolar *et al.* (1994). These approaches are based on time delayed feedback (TDF) of the observed signal and take advantage of the embedded unstable periodic orbits on a chaotic attractor to reduce the control energy cost. This controller and its variations are applied in various electrical systems on the literature, but only a few works focus on mechanical applications and the use of smart materials (Bessa et al., 2009; de Paula and Savi, 2009, 2011; de Souza and Caldas, 2004a; Leiva and Briozzo, 2006). The use of this kind of control can be exploited in different mechanical systems including non-smooth systems (Battelli and Feckan, 2013; de Souza and Caldas, 2004b; Savi *et al.*, 2007), smart material systems (Savi, 2015), machining (Litak *et al.*, 2009a, 2009b), among others.

Smart materials have remarkable properties given by the interaction between different physical fields. This coupling allows an adaptive behavior of systems built with these materials making them specially interesting for control purposes. Shape memory alloys (SMAs) constitute an example of this class of material presenting interesting properties for applied dynamics (Savi, 2015), vibration control (Bessa *et al.*, 2013), origami structures (Kuribayashi *et al.*, 2006), robotics (Kim *et al.*, 2006) and energy harvesting (Lebedev *et al.*, 2011), showing a broad use and potential for a variety of applications. The unique behavior of SMAs is due to its thermomechanical coupling in phase transformations that imply some of their traditional effects as shape memory and pseudoelasticity. The first is the ability to completely recover a residual strain by a proper thermomechanical loading process. The other is a complete strain recovery of the material with a large hysteresis in a loading-unloading cycle.

This work deals with the nonlinear dynamics of an SMA-Pendulum composed of a nonlinear pendulum coupled with SMA springs. This system presents chaotic responses and adaptive behavior, presenting a temperature dependent response. Dynamical investigation is carried out and the extended time delay feedback method (Socolar *et al.*, 1994) is employed for chaos control purposes showing a potential application of SMA in this type of control. Temperature is employed as a control parameter considering asymmetric heat-cooling speeds on a zero dimensional model. Numerical simulations show that the controller is able to stabilize the UPO.

SMA-PENDULUM DYNAMICS

Consider a nonlinear pendulum system (Figure 1) formed by a disc of diameter D(1), and a lumped mass m (2). The excitation is provided by a DC motor (7) with an arm length b, connected to a string-spring system. The spring is made of SMA providing an adaptive behavior to the system. The excitation system has two springs (6) connected by a string.

In one end the first string is connected to the DC motor and in the other end to a spring which involves a disc of diameter d and is connected to one end of the second spring. The other end of the second spring is connected to a linear mechanical actuator which can be used as an anchor as well (5). A magnetic device provides a controlled dissipation to the apparatus (3). A similar system is presented by De Paula *e al.* (2006) and is displayed on Figure 1.

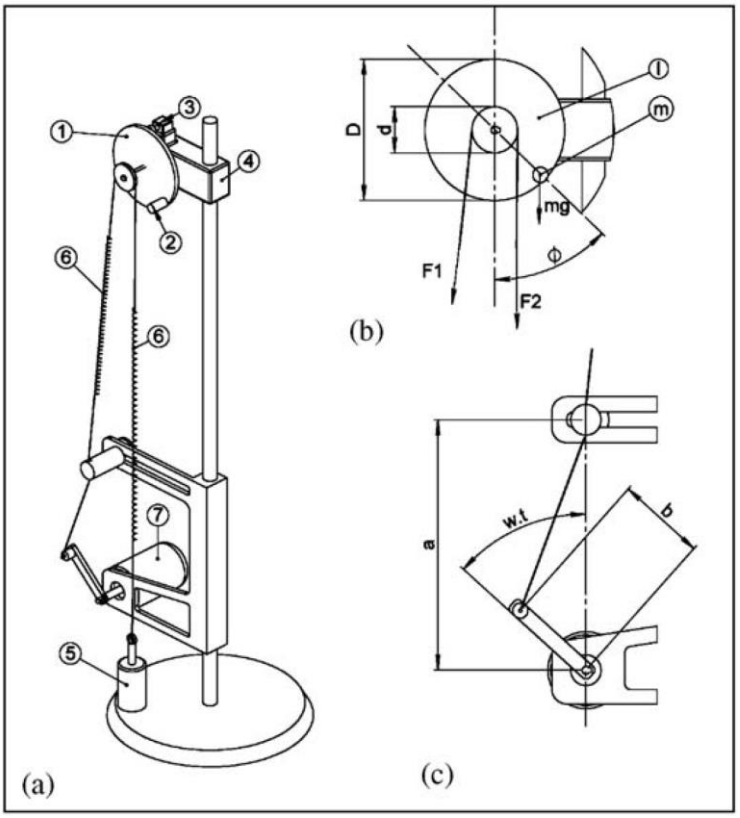

Figure 1 – Nonlinear pendulum: a) physical model (1) metallic disc; (2) lumped mass; (3) magnetic damping device; (4) rotary motion sensor; (5) anchor or mechanical arm; (6) SMA springs; (7) electric motor; b) Parameters and forces on the metallic disc; c) Parameters for driving device (de Paula et al., 2006)**.**

By considering that ϕ is the angle of the pendulum, and assuming that the dissipation is a combination of linear viscous and dry friction, the equation of motion is given by:

$$\phi'' = f(\phi, \phi', t) = -\frac{\vartheta}{I\omega_0}\phi' - \frac{\mu}{mgD}\text{sgn}(\phi') - \frac{\sin(\phi)}{2} + \frac{d}{2mgD}(F_m - s_m) \tag{1}$$

where I is the angular inertia of the pendulum, g is the acceleration of gravity, and ω_0 is a reference frequency defined as follows,

$$\omega_0 = \sqrt{\frac{mgd}{I}} \tag{2}$$

Time derivative $(\,)'$ is related to a dimensionless time defined by $t^* = t\omega_0$. Moreover, s_m is the force of the anchored spring and F_m is the excitation force of the motor-string-spring system.

The displacement due to the movement of the motor can be given as:

$$y = \sqrt{\left(a^2 + b^2 - 2ab\,cos\left(\frac{\omega t^*}{\omega_0} + \theta\right)\right)} - (a - b) - \frac{d\phi}{2} \tag{3}$$

where a is the distance between the center of the disc and the center of the rotor, θ is the initial phase of the motor, ω is the excitation frequency and b is the motor arm length.

Different models are proposed to describe the thermomechanical behavior of SMAs (Lagoudas, 2008; Paiva *et al.*, 2005), and specifically for springs (Aguiar *et al.*, 2010; Enemark *et al.*, 2016). For the sake of simplicity, a polynomial

model is employed following the stress-strain (σ-ε) relation given by,

$$\sigma = a_m^*(T - T_M)\varepsilon - b_m^*\varepsilon^3 + \frac{{b_m^*}^2}{a_m^*(T_A - T_M)}\varepsilon^5 \tag{4}$$

where a_m^* and b_m^* are material parameters, T_M is the temperature below which only martensitic phase is stable, T_A is the temperature above which only austenitic phase is stable (at stress-free scenario), T is the temperature of the SMA. Based on that, and assuming that phase transformation is homogeneous for the spring cross-section, it is possible to write a force-displacement equation for each spring that is formally similar to this stress-strain expression (Aguiar *et al.*, 2010). Hence, for spring 1:

$$F_m(T_1, y) = a_m(T_1 - T_m)y - b_m y^3 + \frac{{b_m}^2}{a_m(T_A - T_m)}y^5 \tag{5}$$

Where T_1 is the temperature on spring 1. And for spring 2, where T_2 is the temperature on the spring:

$$s_m(T_2, \phi) = a_m(T_2 - T_m)\frac{\phi d}{2} - b_m\left(\frac{\phi d}{2}\right)^3 + \frac{{b_m}^2}{a_m(T_A - T_m)}\left(\frac{\phi d}{2}\right)^5 \tag{6}$$

Concerning controller, two possible accessible parameters are treated. The first one is a mechanical controller where the string length that is altered by a step motor, (5) in Figure 1. The second one is a thermal controller where current i_c on the first spring is altered, imposing a temperature change through the joule effect.

The control force F_c is introduced to the system by just one of the parameters and can be added to the pendulum function. Initially, mechanical controller is presented being associated with the following equation of motion:

$$\phi'' = f(\phi, \phi', t^*, \mathrm{l}_0) + \frac{1}{mgD}F_{mec}(\Delta l) \tag{8}$$

where l_0 is a reference length of the string. Length variation Δl is the goal of the actuator resulting in the following actuation force:

$$F_{mec} = \frac{d}{2}\left(a_m(T_1 - T_m)\left(\frac{\phi d}{2} - \Delta l\right) - b_m\left(\frac{\phi d}{2} - \Delta l\right)^3 + \frac{{b_m}^2}{a_m(T_A - T_m)}\left(\frac{\phi d}{2} - \Delta l\right)^5 - F_m\right) \tag{10}$$

Since this is a fifth polynomial there can be five solutions to Δl. To eliminate this ambiguity it is chosen the position that minimizes the consumed energy given by (E_T):

$$E_{\mathrm{m}} = \int_{\mathrm{t_0}}^{\mathrm{t_f}} \frac{F_{mec}(t^*)\Delta \mathrm{l}'(\mathrm{t}^*)}{\omega_0} dt^* \tag{11}$$

where t_0 is the dimensionless time in which the controller starts to move to the target position, t_f is the dimensionless final time and the dot upper script means a time derivative.

Thermal controller can be expressed by the equation of motion presented in the sequence:

$$\phi'' = f(\phi, \phi', t^*, T_0) + \frac{1}{mgD}F_{thermal}(T_c) \tag{9}$$

where T_0 is a reference temperature, and T_c is the imposed temperature by the controller to satisfy $F_{thermal} = F_c$. Thermal actuator provides a force by a change in temperature, being given by:

$$F_{thermal} = \frac{d}{2}a_m\big((T_c(t^*) - T_0)y\big) \tag{12}$$

Thermal controller is limited by heat transfer issues, and therefore, it is restricted by the energy equation. By considering that the ambient functions as a thermal bath, the SMA spring has a constant resistance, is homogeneous in its properties and temperature, and all the heat is produced by the Joule effect:

$$\dot{T_1'} = -\frac{\omega_0 h}{c_p}\left(T_1 - T_{inf}\right) + \frac{\omega_0 i^2 R}{c_p} \tag{13}$$

where T_{inf} is the ambient temperature, i is the current on the spring, R is the spring's resistance, c_p is the spring's thermal capacitance and h is the thermal dissipation coefficient caused by convection. Note that energy equation imposes constraints in two different ways: by allowing just temperatures above T_{inf} to be assessed limiting the values of the force produced by the actuator; and the equation has a characteristic time given by $\omega_0 h/c_p$ which limits how fast the actuator can respond to changes on its value on cooling. Under these assumptions, $F_c(t) = F_{thermal}(t)$ does not hold for all t, introducing an error er on the control force of the form:

$$F_{thermal} = F_c + er(T_1 - T_c) \tag{13}$$

where,

$$er(T_c - T_1) = \frac{d}{2} a_m\left((T_1(t^*) - T_c(t^*))y\right) \tag{14}$$

The energy consumed (E_T) by the control is given by:

$$E_T = \int_{t_0}^{t_f} \frac{i^2 R}{\omega_0} dt^* \tag{15}$$

Dynamics and Unstable Periodic Orbits

Numerical simulations are carried out employing a Fourth-order Runge-Kutta method. Lyapunov exponents are calculated using the algorithm proposed by Wolf *et al.* (1985). Employed parameters are the following: $m = 1.47$ kg, $D = 9.5$ cm, $d = 4.8$ cm, $b = 1.5$ cm, $a = 16$ cm, $\mu = 1.272\ 10^{-4}$ Nm, $\vartheta = 2.368\ \frac{\text{kgm}^2}{\text{s}}$, $g = 9.81\ \text{m/s}^2$, $T_0 = 285.15\ K$ and $\omega = 8.5\ rad/s$. SMA parameters are adjusted with experimental data: $T_A = 289.35$ K, $T_M = 282.45$ K, $a_m = 0.4375$ N/mK and $b_m = 150$ Pa/m, and thermal parameters are adjusted to $h = 2\ W/K$, $c_p = 5\ J/K$ and $R = 100\ \Omega$.

Under these assumptions, the system presents a chaotic response shown on Fig. 2, with a positive Lyapunov exponent of 2.52±0.05 bit/s. The system also presents other orbits coexisting with a chaotic attractor, as is observed in the bifurcation diagram presented in Fig. 3. The system also presents other orbits coexisting with a chaotic attractor. Bifurcation diagram presented in Fig. 3 shows the general scenario of multistable orbits. The diagram is constructed by eliminating the first 700 periods and initializing on different initial positions always with null velocity. The diagram displays an upper chaotic attractor represented by red circles around 6.5 rad/s and a lower chaotic attractor around 8.5 rad/s (blue triangles). In addition, other coexisting periodic orbits are also observed.

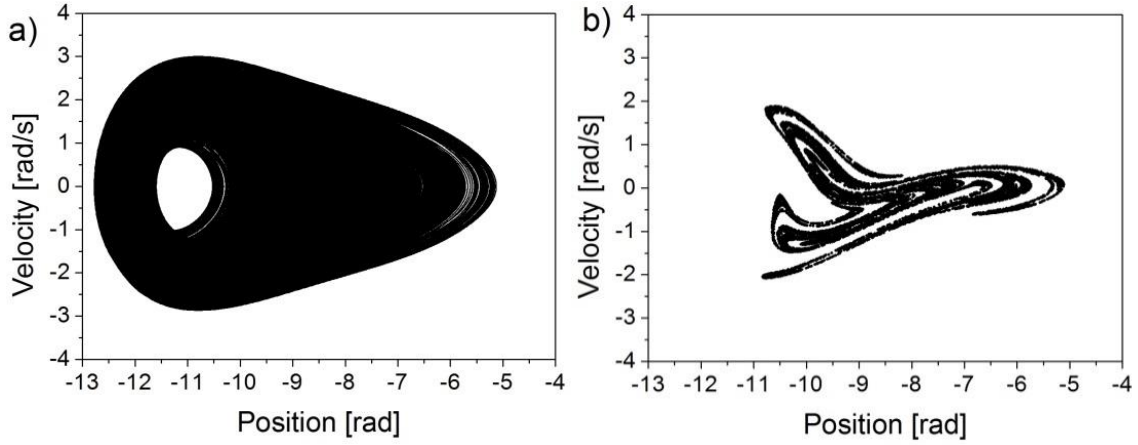

Figure 2 – a) Position time response. b) Poincaré section of the strange attractor with initial condition -6 rad.

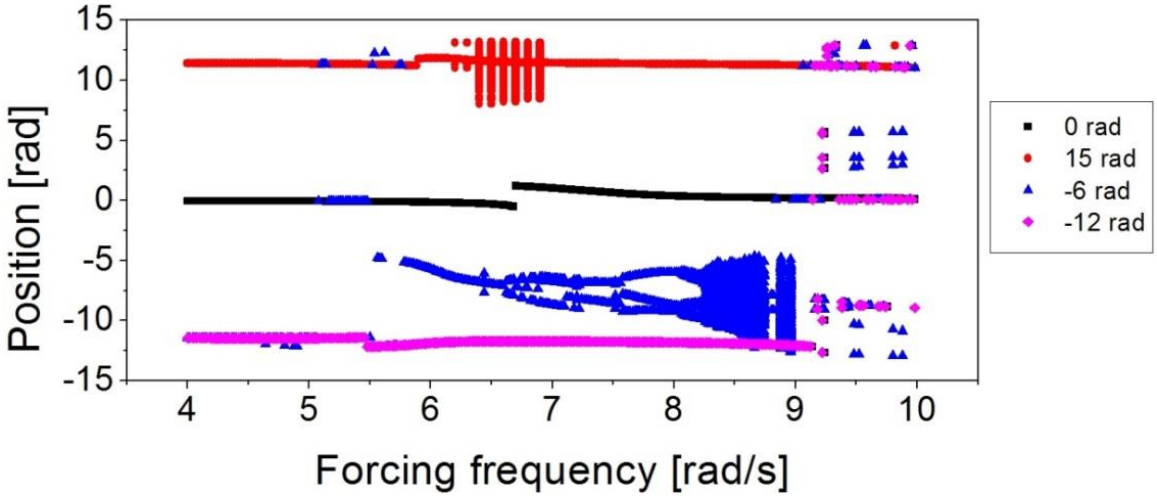

Figure 3 – Bifurcation diagram of position against forcing frequency. Each color represents a coexisting solution of the system. Vertical clusters may indicate chaotic behavior latter confirmed by Lyapunov exponents.

Unstable periodic orbits embedded on the chaotic attractor are extracted by the algorithm proposed by Auerbach *et al.* (1987). The idea is to separate close return points of period $n\tau$ on the Poincaré section within a certain Cartesian radius $r_1 = 0.04$, and separate afterwards different orbits with the same period by another distances $r_2 = 0.15 > r_1$. Several orbits are identified ranging from period 1 to period 14. Some of them are shown in Fig. 4.

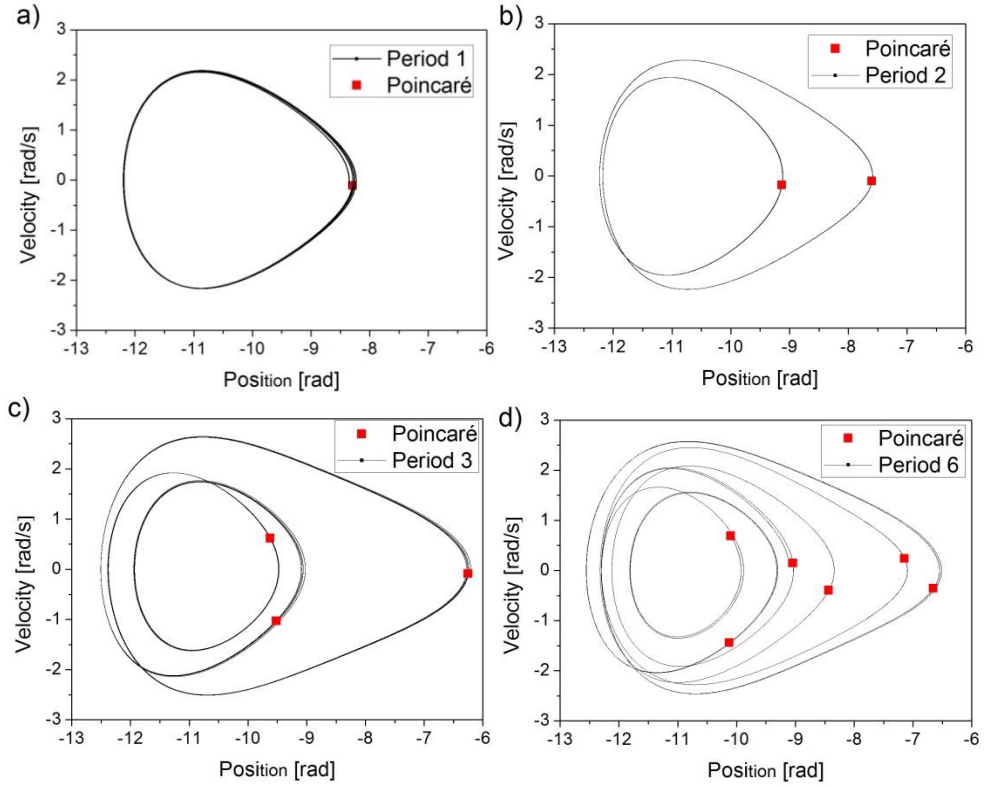

Figure 4 – Identified unstable periodic orbits. a) Period 1, b) Period 2, c) Period 3, d) Period 6.

EXTENDED TIME DELAY FEEDBACK CONTROL

The control strategy is to implement extended time delayed feedback controller (ETDF) on the system, following the equations:

$$F_c = k\big((1-R)S_m - \phi(t)\big) \tag{16}$$

$$S_m = \sum_{j=1}^{\infty} r^{j-1}\phi(t - j\tau_n) \tag{17}$$

where r and k are scalar control parameters and τ_n is the period of the *n*th-periodic UPO to be stabilized. Floquet theory is used to define controller parameters. This theory states that if a perturbation of a periodic orbit of a nonlinear system can be expressed as:

$$\delta\dot{\mathbf{x}} = \mathbf{J}(\mathrm{t})\delta\mathbf{x}(\mathrm{t}) \tag{18}$$

where $\mathbf{J}(\mathrm{t})$ is the Jacobian matrix of the system around the periodic orbit. The perturbation can be given by:

$$\delta\mathbf{x}(t) = \sum_{\mathrm{j}} e^{\mu_j \tau_n}\mathbf{p}_j(t) \tag{19}$$

where $\mathbf{p}_j(t)$ is a periodic function, and μ_i is the j^{th} Floquet exponent that can be extracted from the fundamental matrix $\mathbf{X}(\tau_{\mathrm{n}})$ of a system following the equation:

$$\dot{\mathbf{X}}(\mathrm{t}) = \mathbf{J}(\mathrm{t})\mathbf{X}(\mathrm{t})\ ;\ \ \mathbf{X}(0) = \mathbf{I_0} \tag{20}$$

where $\mathbf{I_0}$ is the identity matrix. After integration of Eq. (20) one can extract the eigenvalues λ_j from $\mathbf{X}(\tau_{\mathrm{n}})$ and obtain the Floquet exponents as:

$$\lambda_j = e^{\mu_j \tau_n} \tag{21}$$

Furthermore, the deviation after a period τ_n is given by:

$$\delta\mathbf{x}(t_0 + \tau_n) = e^{\mu_j \tau_n}\delta\mathbf{x}(\mathrm{t}_0) \tag{22}$$

Based on that, Floquet theory expresses the stability of the periodic orbit and the Floquet multipliers define the system stability when $\mathrm{Re}(\mu_{\max}) < 0$. The orbit is unstable if $\mathrm{Re}(\mu_{\max}) > 0$.

If the system is controlled by the ETDF, the evolution of the fundamental matrix is modified, being given by (Pyragas, 2006):

$$\dot{\mathbf{X}}(\mathrm{t}) = (\mathbf{J}(\mathrm{t}) + \mathrm{g}(\mu_{\mathrm{i}})\mathbf{B})\mathbf{X}(\mathrm{t}) \tag{23}$$

where,

$$\mathrm{g}(\mu) = k\frac{1 - e^{-\mu\tau}}{1 - re^{-\mu\tau}} \tag{24}$$

Considering the pendulum dynamics, **B** is given by:

$$\mathbf{B} = \begin{bmatrix} 0 & 0 \\ -1 & 0 \end{bmatrix} \tag{25}$$

Floquet exponent estimation is associated with the solution of a transcendental equation, Eq. (23), which can be achieved by an iterative method. Table 1 displays the values of Lyapunov exponents, Floquet exponents and the characteristic of some unstable periodic orbits. Note that some UPOs have $\mathrm{Im}(\mu_j)\tau_n = \pi$ indicating that they are formed by finite folds on the state space and are near the edge of the Brillouin zone.

Table 1 – Detected UPOs with respective Floquet and Lyapunov exponents.

	Exponent			
Period	Lyapunov 1	Lyapunov 2	Floquet 1	Floquet 2
N	±0.05 bit/s	±0.05 bit/s	±0.02+0.01i Hz	±0.02+0.01i Hz
1	4.86	-5.04	0.37+0.47i	-0.39+0.47i
2	4.08	-4.25	0.32	-0.34
3	2.81	-2.98	0.22	-0.24
6	2.28	-2.45	0.20+0.08i	-0.21+0.08i
9	2.91	-3.08	0.24	-0.25
12	3.02	-3.19	0.22+0.04i	-0.21+0.04i
14	2.41	-2.58	0.18+0.03i	-0.20+0.03i

The learning stage of the controller is characterized to identify the UPOs and to define controller parameters. Initially, consider the stabilization of a period-1 UPO. Figure 5 displays the Floquet exponents of this UPO against the gain k for various values of r. It can be seen that for values of k above 0.275 the UPO can be stabilized. Note that, for a given r, it is possible to define a region, where the greater Floquet multiplier (μ_{max}) is negative, associated with stable characteristic of the UPO. It starts at $k = k_A$ and ends at $k = k_B$. Within this region, there is an optimal value $k = k_{op}$ related to the minimum value of μ_{max}. The effect of increasing r tends to dislocate the curves to the right bottom corner decreasing the minimum value of the Floquet multiplier (μ_{min}) but also increasing the value of k_{op}.

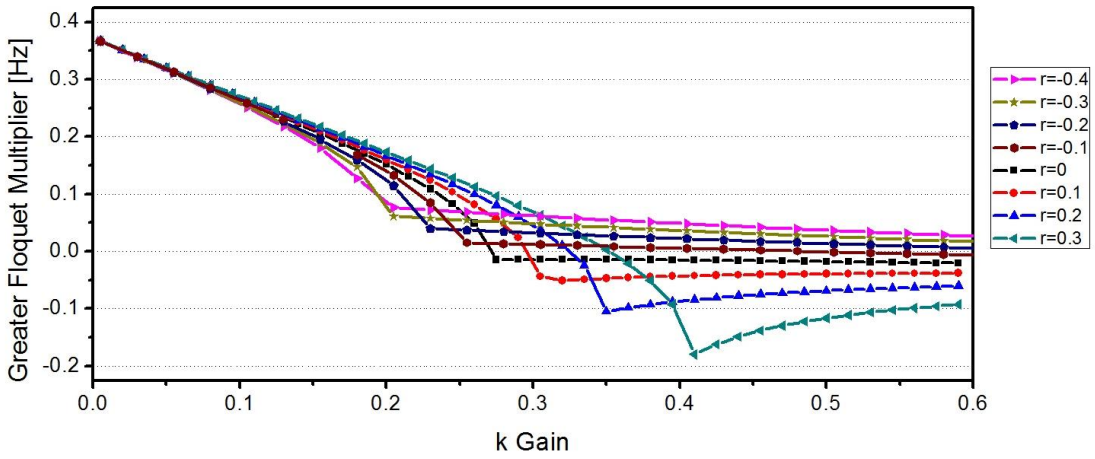

Figure 5 – Maximum Floquet multipliers μ_{max} of the period 1 UPO against k for various values of r.

The pair $k = 0.41$ and $r = 0.3$ presents the lowest minimum exponent value for all the investigated pairs, being chosen as controller parameters to perform UPO stabilization. All tests start with the same initial condition, being inside a chaotic attractor. The control has a wait time of 75 cycles to be initiated.

Mechanical controller is now in focus. Figure 6 displays the system response, control signal and energy consumption for the controller. Note that the system is stabilized at the period-1 UPO consuming a total energy of 136.8 ± 0.1 J and the control signal is very small after a stabilization time $t_s \sim 370\tau_n$.

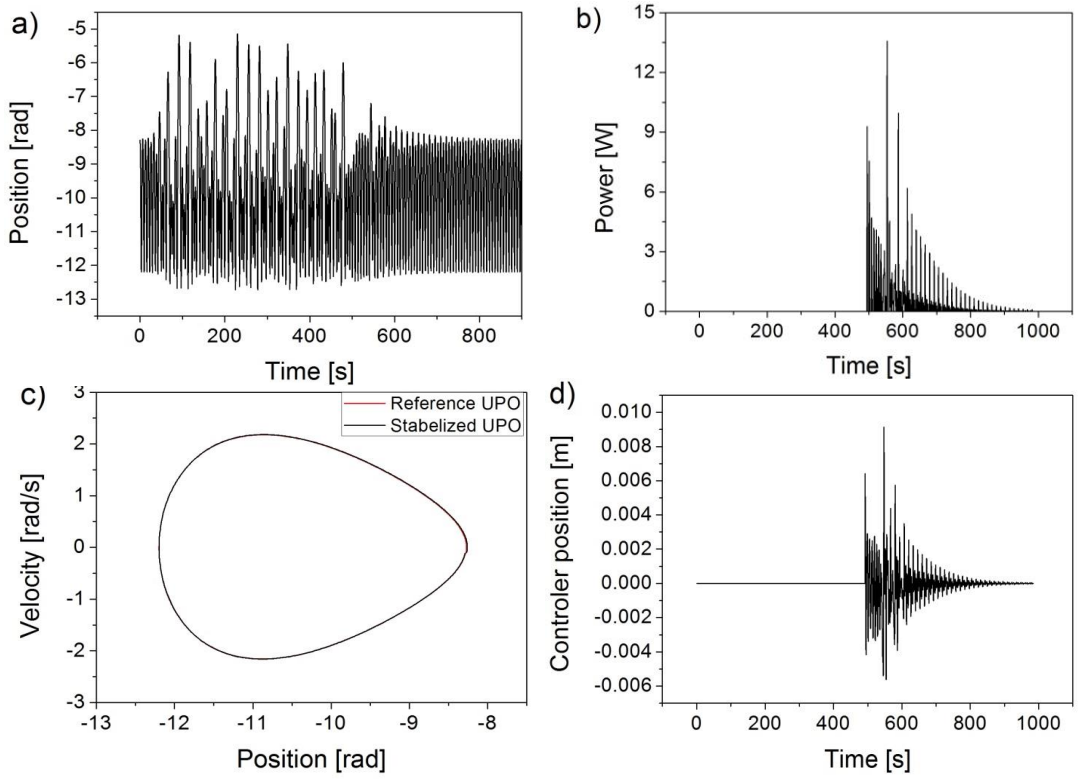

Figure 6 – Mechanical control results. a) Position of the system with time. b) Power consumption of the controller with time. c) Stabilized orbit. d) Controller arm dislocation.

The system is now stabilized by the thermal controller. Ambient temperature is set to be $T_{inf} = 283.15\,K$, two degrees below the reference temperature. This allows the thermal actuator a greater range of accessible forces, but requires a constant reference current i_0 to maintain the spring on T_0 when the control is switched off. Figure 7 presents results for the thermal control showing that the control signal is close to zero after the stabilization. The power consumption is greater than the mechanical control of the previous simulation presenting a value of $1445.4 \pm 0.1\,J$ after excluding the $4000\,J$ needed to maintain the spring on the reference temperature. Moreover, the stabilizing time is lower ($t_s \sim 326\tau_n$) than the mechanical controller. Another important characteristic of the thermal controller is that the cooling process is governed by the energy equation presenting a asymmetric response that can be observed in the detail of Fig. 7d. .

Finally, an analysis of the energy consumption and stabilization time is carried out for different parameters k and r considering the mechanical controller. Figure 8a displays results for different values of r with $k = 0.35$. For $r < -1.8$ the system can not be stabilized indicating the beginning of the instability region. This instability proximity causes a raise on the energy cost due to a decrease on the UPO's stability ($\mu_{max} \sim 0$). As the values of r increases, the influence of the instability region slowly decreases as well as the values of μ_{max}, which can be seen on Fig. 8c. Another effect in the energy cost is the destructive interference of the delayed states for $r < 0$. This causes the total gain on the control to decrease causing the energy cost to go down. These two competitive behaviors explain the vale at negatives values of r. Initially, the first phenomenon predominates giving way to the second until $r = 0.1$. Afterward, the second effect starts to decrease its influence as $r \to 0$. For positive values of r there is no destructive interference and the effect of raising r causes previous states to have more influence on the control, thus increasing the time needed to the control signal to approach zero. Hence, the energy cost tends to decrease as r goes further apart from the instability region until the energy cost starts to increase again due to the increase influence of previous states. The stabilization time follows the same pattern. Finally the behavior of the energy cost is nonlinear indicating that the tuning of r requires a careful analysis of its influence on the system as it may have local minima for the parameter to be optimized.

Figure 8b shows the energy consumption and stabilization time for various values of k, with $r = 0.2$. Once again, it is noticeable the instability region ending at $k = 0.33$ on Fig. 8d. Near these values of k the energy cost and stabilization time are high. Further increasing k, a minimum point is achieved and further increases make the energy cost rise again. Comparing these results with Fig. 8d one can verify that the energy minima is near the lowest Floquet multiplier for the orbit with $r = 0.2$. The stabilization time follows the same behavior of the energy cost but has a minimum after μ_{min} and a flatter valley that starts to increase after the values of k approach the end of the stable region (not displayed at Fig. 8d).

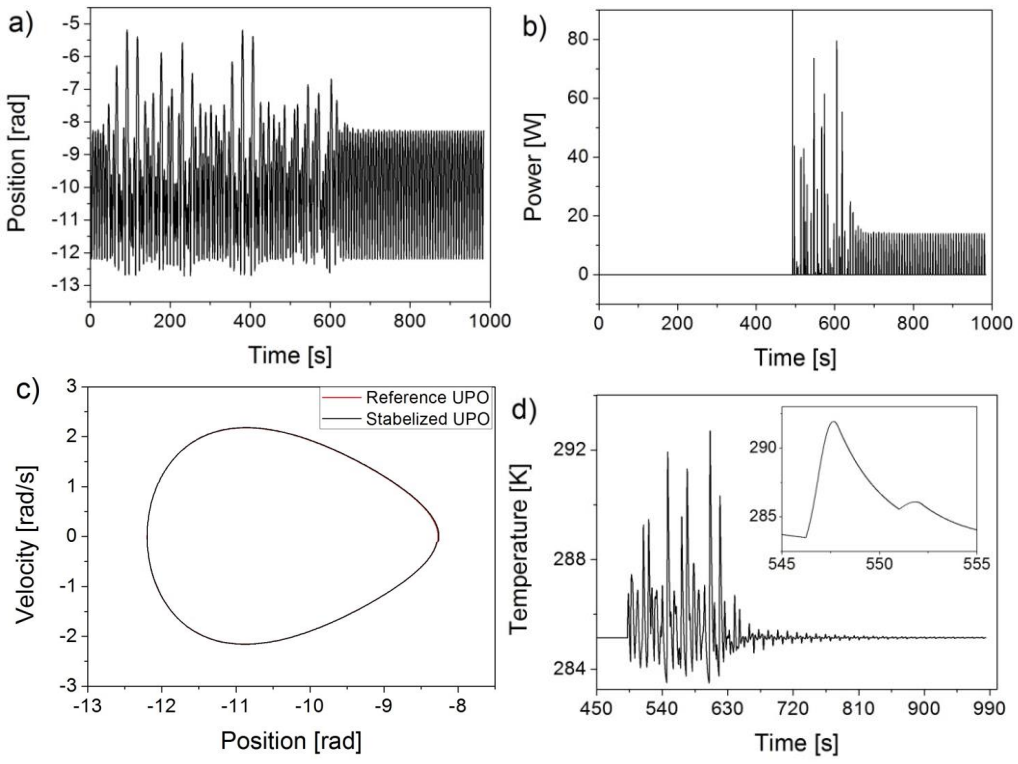

Figure 7 – Thermal control results. a) Position of the system with time. b) Power consumption of the controller with time excluding the current needed to maintain the spring at reference temperature. c) Stabilized orbit. d) Temperature of the spring with highlighted cooling process.

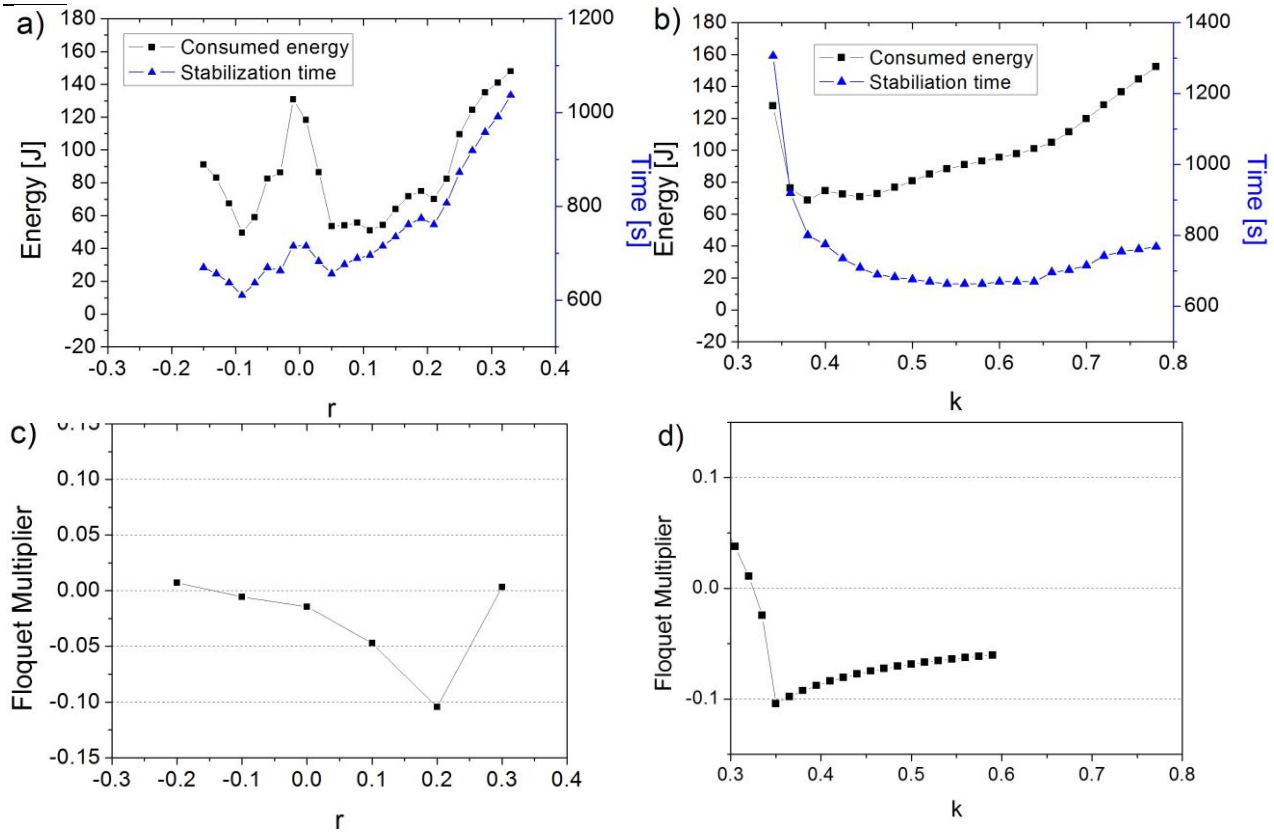

Figure 8 – Energy consumption and stabilization time. a) For various values of r and $k = 0.35$. b) For various values of k and $r = 0.1$. c) Floquet exponents for values of r and $k = 0.35$. D) Floquet exponents for various values of k and $r = 0.1$.

CONCLUSIONS

This work analyzes an SMA pendulum system dynamics. ETDF method is employed for chaos control using the Floquet theory to adjust its parameters. Mechanical and thermal controllers are treated respectively considering a variation of string length and temperature changes on SMA spring. The asymmetry between heating and cooling is incorporated in the controller guided by energy equation analysis. Results show that the mechanical approach presents a greater stabilization time but consumed less energy. On the other hand, thermal control needs to have an ambient temperature lower than the reference temperature requiring greater energy consumption. Finally, an analysis of energy consumption and stabilization time is performed for different controller parameters.

ACKNOWLEDGMENTS

The authors would like to thank the Brazilian Research Agencies CNPq and FAPERJ and through the INCT-EIE (National Institute of Science and Technology - Smart Structures in Engineering) the CNPq and FAPEMIG for their support. The Air Force Office of Scientific Research (AFOSR) is also acknowledged.

REFERENCES

Aguiar, R.A.A., Savi, M.A., Pacheco, P.M.C.L., 2010. Experimental and numerical investigations of shape memory alloy helical springs. Smart Mater. Struct. 19, 25008. doi:10.1088/0964-1726/19/2/025008

Auerbach, D., Cvitanović, P., Eckmann, J.-P., Gunaratne, G., Procaccia, I., 1987. Exploring chaotic motion through periodic orbits. Phys. Rev. Lett. 58, 2387.

Battelli, F., Feckan, M., 2013. Chaos in Forced Impact Systems. Discrete Contin. Dyn. Syst.- Ser. S 6, 861–890. doi:10.3934/dcdss.2013.6.861

Bessa, W.M., de Paula, A.S., Savi, M.A., 2013. Adaptive fuzzy sliding mode control of smart structures. Eur. Phys. J. Spec. Top. 222, 1541–1551. doi:10.1140/epjst/e2013-01943-7

Bessa, W.M., de Paula, A.S., Savi, M.A., 2009. Chaos control using an adaptive fuzzy sliding mode controller with application to a nonlinear pendulum. Chaos Solitons Fractals 42, 784–791. doi:10.1016/j.chaos.2009.02.009

Chen, L., Sun, X., Jiang, H., Xu, X., 2014. A High-Performance Control Method of Constant -Controlled Induction Motor Drives for Electric Vehicles. Math. Probl. Eng. 2014, 1–10. doi:10.1155/2014/386174

de Paula, A.S., Savi, M.A., 2011. Comparative analysis of chaos control methods: A mechanical system case study. Int.

J. Non-Linear Mech. 46, 1076–1089. doi:10.1016/j.ijnonlinmec.2011.04.031
de Paula, A.S., Savi, M.A., 2009. Controlling chaos in a nonlinear pendulum using an extended time-delayed feedback control method. Chaos Solitons Fractals 42, 2981–2988. doi:10.1016/j.chaos.2009.04.039
de Paula, A.S., Savi, M.A., Pereira-Pinto, F.H.I., 2006. Chaos and transient chaos in an experimental nonlinear pendulum. J. Sound Vib. 294, 585–595. doi:10.1016/j.jsv.2005.11.015
de Souza, S.L.T., Caldas, I.L., 2004a. Controlling chaotic orbits in mechanical systems with impacts. Chaos Solitons Fractals 19, 171–178. doi:10.1016/S0960-0779(03)00129-2
de Souza, S.L.T., Caldas, I.L., 2004b. Calculation of Lyapunov exponents in systems with impacts. Chaos Solitons Fractals 19, 569–579. doi:10.1016/S0960-0779(03)00130-9
Enemark, S., Santos, I.F., Savi, M.A., 2016. Modelling, Characterisation and Uncertainties of Stabilised Pseudoelastic Shape Memory Alloy Helical Springs. J. Intell. Mater. Syst. Struct.
Ju, F., Choo, Y.S., Cui, F.S., 2006. Dynamic response of tower crane induced by the pendulum motion of the payload. Int. J. Solids Struct. 43, 376–389. doi:10.1016/j.ijsolstr.2005.03.078
Kim, B., Lee, M.G., Lee, Y.P., Kim, Y., Lee, G., 2006. An earthworm-like micro robot using shape memory alloy actuator. Sens. Actuators Phys. 125, 429–437. doi:10.1016/j.sna.2005.05.004
Kuribayashi, K., Tsuchiya, K., You, Z., Tomus, D., Umemoto, M., Ito, T., Sasaki, M., 2006. Self-deployable origami stent grafts as a biomedical application of Ni-rich TiNi shape memory alloy foil. Mater. Sci. Eng. A 419, 131–137. doi:10.1016/j.msea.2005.12.016
Lagoudas, D.C., 2008. Shape Memory Alloys, 1st ed. Springer US, Boston, MA.
Lebedev, G.A., Gusarov, B.V., Viala, B., Delamare, J., Cugat, O., Lafont, T., Zakharov, D.I., 2011. Thermal energy harvesting using shape memory/piezoelectric composites, in: Solid-State Sensors, Actuators and Microsystems Conference (TRANSDUCERS), 2011 16th International. IEEE, pp. 669–670.
Leiva, A.M., Briozzo, C.B., 2006. Control of chaos and fast periodic transfer orbits in the Earth–Moon CR3BP. Acta Astronaut. 58, 379–386. doi:10.1016/j.actaastro.2005.12.006
Litak, G., Sen, A.K., Syta, A., 2009a. Intermittent and chaotic vibrations in a regenerative cutting process. Chaos Solitons Fractals 41, 2115–2122. doi:10.1016/j.chaos.2008.08.018
Litak, G., Syta, A., Wiercigroch, M., 2009b. Identification of chaos in a cutting process by the 0–1 test. Chaos Solitons Fractals 40, 2095–2101. doi:10.1016/j.chaos.2007.09.093
Monroe, R.J., Shaw, S.W., 2013. Nonlinear Transient Dynamics of Pendulum Torsional Vibration Absorbers—Part I: Theory. Jounrla Vib. Acoust. 135. doi:10:1115/1.4007561
Paiva, A., Savi, M.A., Braga, A.M.B., Pacheco, P.M.C.L., 2005. A constitutive model for shape memory alloys considering tensile–compressive asymmetry and plasticity. Int. J. Solids Struct. 42, 3439–3457. doi:10.1016/j.ijsolstr.2004.11.006
Pan, Y., Zhou, Y., Sun, T., Er, M.J., 2013. Composite adaptive fuzzy H∞ tracking control of uncertain nonlinear systems. Neurocomputing 99, 15–24. doi:10.1016/j.neucom.2012.05.011
Pyragas, K., 2006. Delayed Feedback Control of Chaos. Phylosophical Trans. R. Soc. 364, 2309–2334.
Pyragas, K., 1992. Continuous Control of Chaos by Self-Controlling Feedback. Phys. Lett. A 170, 421–428.
Savi, M.A., 2015. Nonlinear dynamics and chaos in shape memory alloy systems. Int. J. Non-Linear Mech. 70, 2–19. doi:10.1016/j.ijnonlinmec.2014.06.001
Savi, M.A., Divenyi, S., Franca, L.F.P., Weber, H.I., 2007. Numerical and experimental investigations of the nonlinear dynamics and chaos in non-smooth systems. J. Sound Vib. 301, 59–73. doi:10.1016/j.jsv.2006.09.014
Socolar, J.E.S., Sukow, D.W., Gauthier, D.J., 1994. Stabilizing unstable periodic orbits in fast dynamical systems. Phys. Rev. E 50, 3245–3248.
Suzuki, Y., Nomura, T., Casadio, M., Morasso, P., 2012. Intermittent control with ankle, hip, and mixed strategies during quiet standing: A theoretical proposal based on a double inverted pendulum model. J. Theor. Biol. 310, 55–79. doi:10.1016/j.jtbi.2012.06.019
Wolf, A., Swift, J.B., Swinney, H.L., Vastano, J.A., 1985. Determining Lyapunov Exponents From a Time Series. Phys. D 16, 285–317.

RESPONSIBILITY NOTICE

The authors are the only responsible for the material included in this paper.